High Figure-of-Merit Lamb Wave Resonators Based on $Al_{0.7}Sc_{0.3}N$ Thin Film

Shuai Shao, Zhifang Luo, *Student Member, IEEE*, and Tao Wu, *Member, IEEE*

***Abstract*— This work reports the Lamb wave resonator based on $Al_{0.7}Sc_{0.3}N$ thin films using magnetron sputtering with a single alloy target. The resonator fabrication process based on high Sc doping concentration is discussed. $Al_{0.7}Sc_{0.3}N$ thin films with a 1.2° (0002) rocking curve were obtained with improved crystalline quality and reduced abnormal orientation grains (AOGs). The etching process has been optimized to achieve an etch rate of 127 nm/min and a profile angle of 72°. The dispersion properties of Lamb waves and the influence of different electrode metals on the coupling coefficient in $Al_{0.7}Sc_{0.3}N$ thin films were simulated. $Al_{0.7}Sc_{0.3}N$ Lamb wave resonators operating at approximately 300 MHz and 600 MHz were fabricated. A high electromechanical coupling coefficient (k_t^2) of 7.74% is reported, with the loaded quality factor of 1119, respectively. A high Figure-of-Merit (FOM) of 86.6 has been achieved for AlScN film based Lamb wave resonators below 1 GHz. The application potential of high scandium concentration (>25%) in resonators and filters is demonstrated.**

***Index Terms*— Aluminum scandium nitride, $Al_{0.7}Sc_{0.3}N$, lamb wave resonator, piezoelectric, high $k_t^2 \cdot Q$ product.**

I. Introduction

THE emerging 5G application requires high-performance filters with wide bandwidth and low insertion loss for wireless communication devices. High electromechanical coupling coefficients (k_t^2) and quality factors (Q) are the main specifications for resonators. Surface acoustic wave resonators (SAW) based on single crystal piezoelectric material and thin film bulk acoustic wave resonators (FBAR) based on AlN are successfully applied in RF front-end due to their great performance [1], [2]. However, SAW cannot be integrated with CMOS process and FBAR is difficult to integrate multibands monolithically. Therefore, Lamb wave resonators (LWR) based on aluminum nitride (AlN) with the ability to lithographically define operating frequencies have been a hot topic in the past decade [3]. Many works have been performed in the direction of Q enhancement, energy confinement and higher order modes [4]. Compared with other piezoelectric materials, the low piezoelectric constant of AlN limits the maximum k_t^2 to approximately 6% [5]. Currently, Sc-doped aluminum nitride (AlScN) serves as one of the most promising candidates for improving the coupling coefficient of resonators [6], [7].

Manuscript received July 4, 2021; revised July 21, 2021; accepted July 22, 2021. Date of publication July 26, 2021; date of current version August 26, 2021. This work was supported in part by the ShanghaiTech Quantum Device Lab (SQDL) and the Analytical Instrumentation Center XRD Lab, ShanghaiTech University under Grant SPST-AIC10112914, in part by the National Natural Science Foundation of China under Grant 61874073, and in part by the Natural Science Foundation of Shanghai under Grant 19ZR1477000. The review of this letter was arranged by Editor S. Pourkamali. *(Corresponding author: Tao Wu.)*

The authors are with the School of Information Science and Technology, ShanghaiTech University, Shanghai 201210, China, also with the Shanghai Institute of Microsystem and Information Technology, Shanghai 200050, China, and also with the University of Chinese Academy of Sciences, Beijing 100049, China (e-mail: shaoshuai@shanghaitech.edu.cn; wutao@shanghaitech.edu.cn).

Color versions of one or more figures in this letter are available at https://doi.org/10.1109/LED.2021.3100036.

Digital Object Identifier 10.1109/LED.2021.3100036

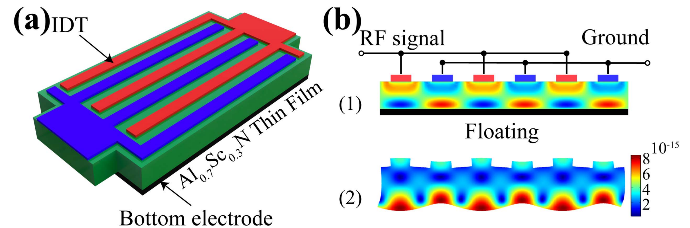

Fig. 1. (a) Illustrations of the lamb wave resonator with floating bottom electrode. (b) Finite Element Analysis (FEA) simulation of the S_0 mode lamb wave resonator. (1) electric potential, (2) total displacement.

A few studies have demonstrated the performance enhancement of AlScN thin film based SAW, FBAR, laterally coupled alternating thickness (LCAT) resonator [8], [9] and LWR resonators [9]–[22]. Due to the overall improvement of piezoelectric coefficients by Sc doping, the electromechanical coupling coefficients of various modes can significantly benefit from it. However, AlScN thin films face the problems of crystalline orientation, defects (AOGs) and huge residual stresses [23]. The large number of defects introduces additional energy loss and causes a decrease in quality factor, which is more significant at high concentrations (>20%). On the other hand, when the Sc concentration increases, the etching difficulty increases significantly [24], [25]. Currently, less work has been done for Lamb wave resonant devices with Sc concentration higher than 25%, and this work breaks through the process challenges.

In this work, we report the design and experimental results of lamb wave resonators based on 1 μm $Al_{0.7}Sc_{0.3}N$ thin films. By optimizing the sputtering process, $Al_{0.7}Sc_{0.3}N$ films with a balance of crystalline quality and residual stress were obtained. The inductively coupled plasma (ICP) etch rate for $Al_{0.7}Sc_{0.3}N$ was effectively enhanced by increasing the RF power with a balance of the selectivity and sidewall profile. Simulations are performed for the Lamb wave propagation and piezoelectric coupling characteristics of $Al_{0.7}Sc_{0.3}N$ thin film and high FOM Lamb wave resonator devices have demonstrated below 1 GHz.

II. Design and Fabrication

As shown in Fig. 1 (a), the Lamb wave resonator device consists of a floating bottom metal, 1 μm $Al_{0.7}Sc_{0.3}N$ thin film and top interdigitated (IDT) electrodes. To obtain a better crystalline quality of the AlScN thin film, 100 nm platinum (Pt) is used for the bottom floating metal and

0741-3106 © 2021 IEEE. Personal use is permitted, but republication/redistribution requires IEEE permission.
See https://www.ieee.org/publications/rights/index.html for more information.

Authorized licensed use limited to: ShanghaiTech University. Downloaded on June 01,2023 at 06:29:33 UTC from IEEE Xplore. Restrictions apply.

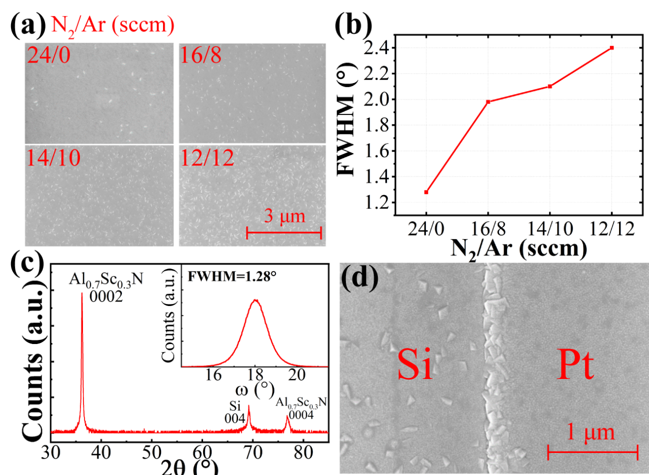

Fig. 2. (a) SEM and (b) rocking curve of $Al_{0.7}Sc_{0.3}N$ surface with different N_2/Ar sputtering gas ratio. (c) X-ray diffraction $2\theta/\theta$ scan $Al_{0.7}Sc_{0.3}N$ and rocking curve of $Al_{0.7}Sc_{0.3}N$ (0002) with 24 sccm N_2 (inset). (d) SEM image of $Al_{0.7}Sc_{0.3}N$ grown on Si and Pt surfaces.

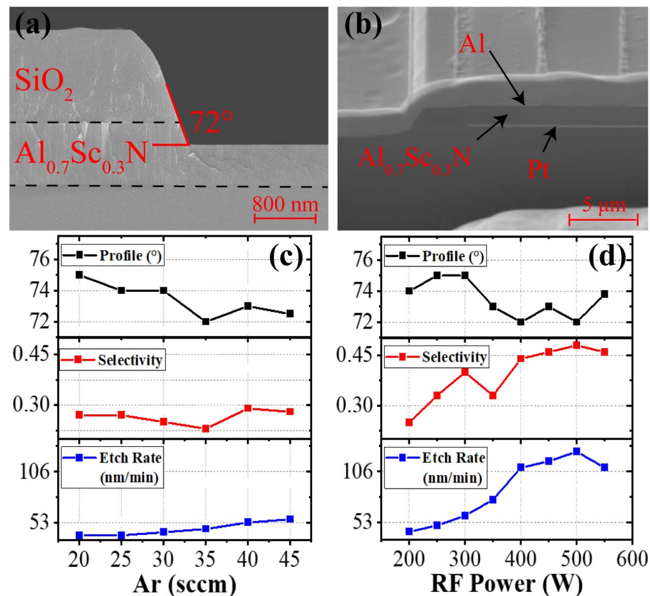

Fig. 3. SEM image of $Al_{0.7}Sc_{0.3}N$ film (a) 72° etching profile at RF power of 500 W, (b) cross section view by focused ion beam (FIB) process. The etch rate, etching profile and selectivity ratio against SiO_2 as a function of (c) Ar flow rate, and (d) RF power.

200 nm aluminum (Al) is used for the top IDT electrodes to reduce mass loading and resistance loss. Fig. 1 (b) shows the corresponding electric potential and total displacement in S_0 mode Lamb wave at resonance. The devices were fabricated by a three-layer mask process [26]. ICP etching is performed on the $Al_{0.7}Sc_{0.3}N$ film to define the reflection boundary and release window of the resonators using 4-μm-thick SiO_2 as a hard mask.

Firstly, 1 μm thick $\mathbf{Al_{0.7}Sc_{0.3}}$N thin film was deposited on 4-inch silicon wafers (100) using a pulsed DC magnetron reactive sputtering in the EVATEC CLN200 MSQ with single 4-inch $Al_{0.7}Sc_{0.3}$ alloy target. As shown in Fig. 2 (a) and (b), the ratio of N_2/Ar significantly affects the crystal quality of AlScN films. Ar as a commonly used sputtering gas and a stress control method is not suitable in AlScN film deposition. Larger Ar ratios add large amounts of AOGs and cause a decrease in full width at half maximum (FWHM), which will directly lead to a deterioration of the piezoelectric coefficient. As shown in Fig. 2 (c), the FWHM of $Al_{0.7}Sc_{0.3}N$ (0002) is 1.28°. Nice crystal orientation was obtained by using pure N_2 as process gas. To prevent excessive stress of the film causing a damage to the device after release, a better average stress of 67.13 MPa and a stress range of 47.06 MPa over a 4-inch wafer were obtained (Toho FLX2320) due to a better stress control in single alloy sputtering than co-sputtering [12]. In addition, Fig. 2 (d) shows the defect of $\mathbf{Al_{0.7}Sc_{0.3}}$N film grown on Si and Pt two different surfaces. Pt has been shown to provide a good growth interface for AlN [27]. Symmetrical properties similar to sapphire allow AlScN nucleation on Pt in a tight arrangement. Here, less AOGs were observed on the Pt surface, making Pt thin film as preferred bottom electrode material for high quality $\mathbf{Al_{0.7}Sc_{0.3}}$N deposition.

Secondly, a series of experiments were carried out to increase etch rate in the ICP etching process (Leuven Instrument HAASRODE-E200A). Fig. 3 (a) and (b) show the etching profile and cross section view by FIB of the optimized ICP process, respectively. Here, the mechanism of etch rate drop is found and solved. $ScCl_3$ is a byproduct produced during AlScN etching, and its volatility is so low that it will cover the etched surface, making it difficult for the Cl_2 reaction gas to react with the AlScN film [28]. Therefore, the method of increasing the rate is the enhance intensity of the physical bombardment and minimize non-volatile $ScCl_3$ byproducts re-deposition. Fig. 3 (c) and (d) show the etch rate, profile and selectivity ratio versus the Ar flow rate and RF power at $BCl_3/Cl_2 = 30/25$ sccm. The Ar gas flow has little impact on the selectivity. When the RF power increases from 200 W to 550 W, both etch rate and selectivity increase significantly due to increased plasma energy. The etch rate increases from about 40 nm/min to 110 nm/min, and the selectivity increases from 0.25 to about 0.46. The increase in plasma energy leads to an increase in the physical bombardment of the etched surface by Ar. The enhancement of physical bombardment could strip $ScCl_3$ from the surface and expose AlScN, indirectly promoting the etch rate.

III. Result and Discussion

Since Sc doping significantly changes the material properties of AlN film, the Lamb wave propagation characteristics based on $Al_{0.7}Sc_{0.3}N$ films need to be re-evaluated. The phase velocity with the normalized thickness ($h_{\mathrm{AlScN}}/\lambda$) is calculated using the Floquet periodicity boundary condition method. The material parameters used in the simulation are shown in Table I [29] and [30]. The difference in phase velocity between the free surface v_0 and the metalized surface v_m is used to estimate the intrinsic coupling coefficient (K^2) [5]. Fig. 4 (a) shows the simulated phase velocities of the S_0 Lamb wave mode in AlN and $Al_{0.7}Sc_{0.3}N$ with the normalized thickness. The materials of the electrodes are Pt and Al, and their thicknesses are fixed at 0.1^*h_{AlScN} and 0.2^*h_{AlScN}, respectively. The S_0 mode phase velocity in $Al_{0.7}Sc_{0.3}N$ film decreases from around 8703 m/s to 7193 m/s in pure AlN film. The simulation results are well fitted to the measurement by taking the mechanical load into account. Fig. 4 (b) shows the influence of different metals on K^2. When the normalized thickness is below 0.1, the Al electrode can obtain the highest coupling coefficient.

Authorized licensed use limited to: ShanghaiTech University. Downloaded on June 01,2023 at 06:29:33 UTC from IEEE Xplore. Restrictions apply.

TABLE I
MATERIAL PARAMETER OF $Al_{0.7}Sc_{0.3}N$

	Value		Value
c_{11} (GPa)	327.67	e_{15} (C/m^2)	-0.32
c_{12} (GPa)	146.91	e_{31} (C/m^2)	-0.72
c_{13} (GPa)	135.40	e_{33} (C/m^2)	2.33
c_{33} (GPa)	232.12	$\varepsilon_{33}^{eff}/\varepsilon_0$	19.6
c_{44} (GPa)	107.94	ρ (kg/m^3)	3319

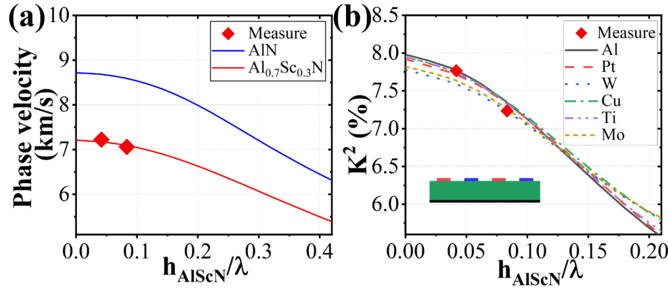

Fig. 4. (a) FEM simulated phase velocities for the S_0 Lamb wave mode with normalized thickness h_{AlScN}/λ. (b) Simulated K^2 of the S_0 mode in the $Al_{0.7}Sc_{0.3}N$ thin films with various metals of top electrodes.

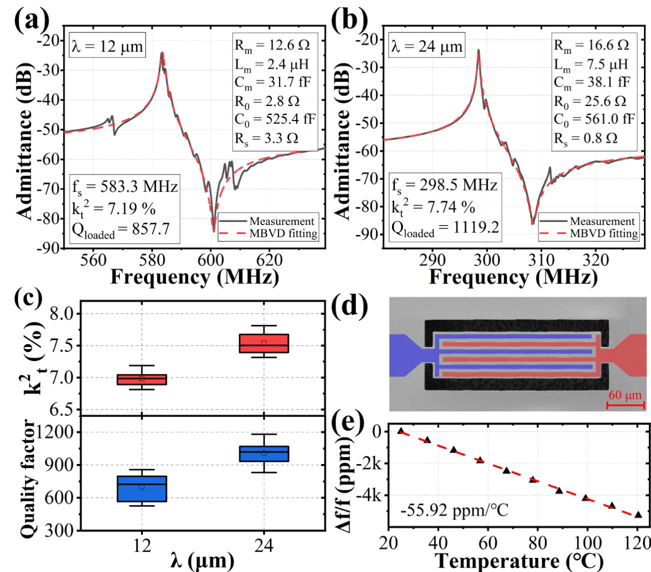

Fig. 5. Measured admittance spectrum of the LWRs with wavelength of (a) 12 μm and (b) 24 μm with the MBVD model parameters. (c) Measured k_t^2 and Q of LWR with $Al_{0.7}Sc_{0.3}N$. (d) SEM of fabricated LWR. (e) Temperature coefficient of frequency (TCF) with $Al_{0.7}Sc_{0.3}N$.

Fig. 5 (a) and (b) show measured admittance frequency response (Keysight PNA-L N5234B) of two fabricated LWRs with the wavelength of 12 μm and 24 μm, respectively. Modified Butterworth-Van Dyke (MBVD) model fitting as well as extracted parameters are displayed in the figures. The resonant frequencies are 583.3 MHz and 298.5 MHz, while k_t^2 are 7.19% and 7.74%, respectively. The measurement results fit well with FEA simulation. Thanks to the optimized $Al_{0.7}Sc_{0.3}N$ film crystalline quality and stress control, the resonator achieves a loaded Q of 1119.2 and low R_m of 16.6 Ω, which leads to a high FOM of approximately 86.6 for 24 μm LWR.

The corresponding measurement results of resonance frequency, Sc doping concentration, k_t^2, Q and FOM ($k_t^2 \cdot Q$) are summarized in Table II with comparison to other works.

TABLE II
COMPARISON WITH PREVIOUS WORKS

Design	Sc (%)	Device	f_s (GHz)	k_t^2 (%)	Q*	FOM ($k_t^2 \cdot Q$)
[12]	43	SAW	1.6	3.8	660	25.1
[25]	40	LWR	2.6	7.4	117	8.7
[20]	32	LWR	0.04	10.3	1184	122
[22]	30	FBAR	2.9	18.1	210	38.0
[21]	28	FBAR	2.47	11.7	689	80.5
[10]	23	LWR	4.9	7.45	94	7.3
[13]	23	SAW	1.7	2.4	538	12.9
[14]	20	LWR	3	6.5	600	39
[17]	20	LWR	0.2	4.5	1240	55.8
[9]	12	LCAT	2.0	10.2	855	87.0
This work	30	LWR	0.3	7.74	1119	86.6

*note: different papers may have different definitions on k_t^2 and Q

FBAR is easier to obtain high FOM due to a larger d_{33}, however, it is challenging to achieve multiple bands monolithically [22], [29]. The LCAT mode utilizes both d_{33} and d_{31} piezoelectric coefficients, and an electromechanical coupling coefficient of more than 10% has been obtained at 12% Sc concentration [9]. LCAT resonators need to pattern the bottom electrode, as shown in Fig. 2 (d), the metal and silicon boundaries could create a large number of defects, which requires significant process control and optimization. When the Sc concentration is more than 20%, it can be observed that the AlScN film based devices have difficulty in achieving high quality factors comparable to pure AlN film, due to intrinsic large ionic vibrations, stress control of AlScN film as well as the device design. Recently, a comparable FOM of 92 has been achieved at $Al_{0.68}Sc_{0.32}N$ film, however, the operating frequency is relatively low since the viscosity of the materials dominates while resonating at high frequencies [20]. The LWR with a floating bottom electrode in this work has the advantage of frequency scaling and tunability as well as easier process integration. By utilizing the array structure and further optimized anchor design, the device can be easily scaled to higher frequencies with 50 Ω impedance matching [31].

In order to investigate the effect of Sc doping on the temperature characteristics of the resonators, temperature measurements in the range of 25 °C to 120 °C were performed. Fig. 5 (e) shows the measured resonance shift as a function of the temperature for 24 μm $Al_{0.7}Sc_{0.3}N$ resonator device. The extracted TCF is −55.92 ppm/°C, which is larger than pure AlN. This attributes to the increased thermal expansion coefficients and reduced elasticity modulus of $Al_{0.7}Sc_{0.3}N$ film with high Sc doping. Further temperature compensation technique could be implemented to improve the device TCF.

IV. CONCLUSION

In this work, we have successfully demonstrated high quality $Al_{0.7}Sc_{0.3}N$ thin film as well as large FOM Lamb wave resonators. By utilizing pure nitrogen, nice crystalline quality and clean surface has been obtained. The k_t^2 of fabricated Lamb wave resonators has been significantly improved to 7.74% with a loaded Q of 1119. Such a high FOM of over 86.6, high quality factor and low R_m in AlScN film based Lamb wave resonators provide wide potential applications in RF communication and sensors by adopting Scandium doping in AlN film, at least at frequencies below 1 GHz.

Authorized licensed use limited to: ShanghaiTech University. Downloaded on June 01,2023 at 06:29:33 UTC from IEEE Xplore. Restrictions apply.

References

[1] R. Lu, Y. Yang, S. Link, and S. Gong, "A1 resonators in 128° Y-cut lithium Niobate with electromechanical coupling of 46.4%," *J. Microelectromech. Syst.*, vol. 29, no. 3, pp. 313–319, Jun. 2020, doi: 10.1109/JMEMS.2020.2982775.

[2] R. Ruby, P. Bradley, J. Larson, Y. Oshmyansky, and D. Figueredo, "Ultra-miniature high-Q filters and duplexers using FBAR technology," in *IEEE Int. Solid-State Circuits Conf. (ISSCC) Dig. Tech. Papers*, Feb. 2001, pp. 120–121, doi: 10.1109/ISSCC.2001.912569.

[3] J. Bjurström, I. Katardjiev, and V. Yantchev, "Lateral-field-excited thin-film Lamb wave resonator," *Appl. Phys. Lett.*, vol. 86, no. 15, Apr. 2005, Art. no. 154103, doi: 10.1063/1.1900312.

[4] V. Yantchev and I. Katardjiev, "Thin film Lamb wave resonators in frequency control and sensing applications: A review," *J. Micromech. Microeng.*, vol. 23, no. 4, Apr. 2013, Art. no. 043001, doi: 10.1088/0960-1317/23/4/043001.

[5] J. Zou, C.-M. Lin, A. Gao, and A. P. Pisano, "The multi-mode resonance in AlN Lamb wave resonators," *J. Microelectromech. Syst.*, vol. 27, no. 6, pp. 973–984, Dec. 2018, doi: 10.1109/JMEMS.2018.2867813.

[6] M. Akiyama, T. Kamohara, K. Kano, A. Teshigahara, Y. Takeuchi, and N. Kawahara, "Enhancement of piezoelectric response in scandium aluminum nitride alloy thin films prepared by dual reactive cosputtering," *Adv. Mater.*, vol. 21, no. 5, pp. 593–596, Dec. 2008, doi: 10.1002/adma.200802611.

[7] M. T. Hardy, B. P. Downey, N. Nepal, D. F. Storm, D. S. Katzer, and D. J. Meyer, "Epitaxial ScAlN grown by molecular beam epitaxy on GaN and SiC substrates," *Appl. Phys. Lett.*, vol. 110, no. 16, Apr. 2017, Art. no. 162104, doi: 10.1063/1.4981807.

[8] N. Wang, Y. Zhu, B. Chen, and Y. Zhang, "Over 12% of coupling coefficient demonstrated by 3 GHz $Sc_{0.12}Al_{0.88}N$ based laterally coupled alternating thickness (LCAT) mode resonators," in *Proc. IEEE Int. Ultrason. Symp. (IUS)*, Oct. 2019, pp. 1971–1973, doi: 10.1109/ULTSYM.2019.8926087.

[9] N. Wang, Y. Zhu, G. L. Chua, B. Chen, S. Merugu, N. Singh, and Y. Gu, "Over 10% of k_{eff}^2 demonstrated by 2-GHz spurious mode-free $Sc_{0.12}Al_{0.88}N$ laterally coupled alternating thickness mode resonators," *IEEE Electron Device Lett.*, vol. 40, no. 6, pp. 957–960, Jun. 2019, doi: 10.1109/LED.2019.2910836.

[10] M. Park and A. Ansari, "Epitaxial $Al_{0.77}Sc_{0.23}N$ SAW and Lamb wave resonators," in *Proc. Joint Conf. IEEE Int. Freq. Control Symp. Int. Symp. Appl. Ferroelectr. (IFCS-ISAF)*, Jul. 2020, pp. 1–3, doi: 10.1109/IFCS-ISAF41089.2020.9234850.

[11] A. Lozzi, E. Ting-Ta Yen, P. Muralt, and L. G. Villanueva, "$Al_{0.83}Sc_{0.17}N$ contour-mode resonators with electromechanical coupling in excess of 4.5%," *IEEE Trans. Ultrason., Ferroelectr., Freq. Control*, vol. 66, no. 1, pp. 146–153, Jan. 2019, doi: 10.1109/TUFFC.2018.2882073.

[12] A. Teshigahara, K.-Y. Hashimoto, and M. Akiyama, "Scandium aluminum nitride: Highly piezoelectric thin film for RF SAW devices in multi GHz range," in *Proc. IEEE Int. Ultrason. Symp.*, Oct. 2012, pp. 1–5, doi: 10.1109/ultsym.2012.0481.

[13] A. Ding, L. Kirste, Y. Lu, R. Driad, N. Kurz, V. Lebedev, T. Christoph, N. M. Feil, R. Lozar, T. Metzger, O. Ambacher, and A. Žukauskaitė, "Enhanced electromechanical coupling in SAW resonators based on sputtered non-polar $Al_{0.77}Sc_{0.23}N$ $11\bar{2}0$ thin films," *Appl. Phys. Lett.*, vol. 116, no. 10, Mar. 2020, Art. no. 101903, doi: 10.1063/1.5129329.

[14] Z. A. Schaffer, G. Piazza, S. Mishin, and Y. Oshmyansky, "Super high frequency simple process flow cross-sectional Lamé mode resonators in 20% scandium-doped aluminum nitride," in *Proc. IEEE 33rd Int. Conf. Micro Electro Mech. Syst. (MEMS)*, Jan. 2020, pp. 1281–1284, doi: 10.1109/MEMS46641.2020.9056279.

[15] M. Park, J. Wang, R. Dargis, A. Clark, and A. Ansari, "Super high-frequency scandium aluminum nitride crystalline film bulk acoustic resonators," in *Proc. IEEE Int. Ultrason. Symp. (IUS)*, Oct. 2019, pp. 1689–1692, doi: 10.1109/ULTSYM.2019.8925598.

[16] B. A. Griffin, M. D. Henry, R. W. Reger, and B. Heinz, "$Sc_xAl_{1-x}N$ film evaluation using contour mode resonators," in *Proc. IEEE Int. Ultrason. Symp. (IUS)*, Sep. 2017, pp. 1–4, doi: 10.1109/ULTSYM.2017.8092391.

[17] L. Colombo, A. Kochhar, C. Xu, G. Piazza, S. Mishin, and Y. Oshmyansky, "Investigation of 20% scandium-doped aluminum nitride films for MEMS laterally vibrating resonators," in *Proc. IEEE Int. Ultrason. Symp. (IUS)*, Sep. 2017, pp. 1–4, doi: 10.1109/ULTSYM.2017.8092076.

[18] S. Rassay, F. Hakim, M. Ramezani, and R. Tabrizian, "Acoustically coupled wideband RF filters with bandwidth reconfigurablity using ferroelectric aluminum scandium nitride film," in *Proc. IEEE 33rd Int. Conf. Micro Electro Mech. Syst. (MEMS)*, Jan. 2020, pp. 1254–1257, doi: 10.1109/mems46641.2020.9056353.

[19] A. Qamar, H.-P. Phan, T. Dinh, N.-T. Nguyen, and M. Rais-Zadeh, "ScAlN/3C-SiC/Si platform for monolithic integration of highly sensitive piezoelectric and piezoresistive devices," *Appl. Phys. Lett.*, vol. 116, no. 13, Mar. 2020, Art. no. 132902, doi: 10.1063/5.0004943.

[20] G. Esteves, T. R. Young, Z. Tang, S. Yen, T. M. Bauer, M. D. Henry, and R. H. Olsson, "$Al_{0.68}Sc_{0.32}N$ Lamb wave resonators with electromechanical coupling coefficients near 10.28%," *Appl. Phys. Lett.*, vol. 118, no. 17, Apr. 2021, Art. no. 171902, doi: 10.1063/5.0047647.

[21] M. Park, J. Wang, and A. Ansari, "High-overtone thin film ferroelectric AlScN-on-silicon composite resonators," *IEEE Electron Device Lett.*, vol. 42, no. 6, pp. 911–914, Jun. 2021, doi: 10.1109/led.2021.3070274.

[22] J. Wang, M. Park, S. Mertin, T. Pensala, F. Ayazi, and A. Ansari, "A film bulk acoustic resonator based on ferroelectric aluminum scandium nitride films," *J. Microelectromech. Syst.*, vol. 29, no. 5, pp. 741–747, Oct. 2020, doi: 10.1109/JMEMS.2020.3014584.

[23] C. S. Sandu, F. Parsapour, S. Mertin, V. Pashchenko, R. Matloub, T. LaGrange, B. Heinz, and P. Muralt, "Abnormal grain growth in AlScN thin films induced by complexion formation at crystallite interfaces," *Phys. Status Solidi (A)*, vol. 216, no. 2, Jan. 2019, 1800569, Art. no. 1800569, doi: 10.1002/pssa.201800569.

[24] M. David Henry, T. R. Young, and B. Griffin, "ScAlN etch mask for highly selective silicon etching," *J. Vac. Sci. Technol. B, Microelectron.*, vol. 35, no. 5, Sep. 2017, Art. no. 052001, doi: 10.1116/1.4994841.

[25] A. Konno, M. Sumisaka, A. Teshigahara, K. Kano, K.-Y. Hashimo, H. Hirano, M. Esashi, M. Kadota, and S. Tanaka, "ScAlN Lamb wave resonator in GHz range released by XeF_2 etching," in *Proc. IEEE Int. Ultrason. Symp. (IUS)*, Jul. 2013, pp. 1378–1381, doi: 10.1109/ULTSYM.2013.0350.

[26] T. Wu, R. Lu, A. Gao, C. Tu, T. Manzaneque, and S. Gong, "A chip-scale RF MEMS gyrator via hybridizing lorentz-force and piezoelectric transductions," in *Proc. IEEE 32nd Int. Conf. Micro Electro Mech. Syst. (MEMS)*, Jan. 2019, pp. 887–890, doi: 10.1109/MEMSYS.2019.8870764.

[27] M.-A. Dubois and P. Muralt, "Stress and piezoelectric properties of aluminum nitride thin films deposited onto metal electrodes by pulsed direct current reactive sputtering," *J. Appl. Phys.*, vol. 89, no. 11, pp. 6389–6395, Jun. 2001, doi: 10.1063/1.1359162.

[28] Z. Luo, S. Shao, and T. Wu, "Characterization of AlN and AlScN film ICP etching for micro/nano fabrication," *Microelectron. Eng.*, vols. 242–243, Apr. 2021, Art. no. 111530, doi: 10.1016/j.mee.2021.111530.

[29] M. A. Caro, S. Zhang, T. Riekkinen, M. Ylilammi, M. A. Moram, O. Lopez-Acevedo, J. Molarius, and T. Laurila, "Piezoelectric coefficients and spontaneous polarization of ScAlN," *J. Phys. Condens. Matter*, vol. 27, no. 24, Jun. 2015, Art. no. 245901, doi: 10.1088/0953-8984/27/24/245901.

[30] N. Kurz, A. Ding, D. F. Urban, Y. Lu, L. Kirste, N. M. Feil, A. Žukauskaitė, and O. Ambacher, "Experimental determination of the electro-acoustic properties of thin film AlScN using surface acoustic wave resonators," *J. Appl. Phys.*, vol. 126, no. 7, Aug. 2019, Art. no. 075106, doi: 10.1063/1.5094611.

[31] C. Cassella, G. Chen, T. Wu, Z. Qian, and M. Rinaldi, "Low impedance arrays of coupled cross-sectional Lamé mode resonators with high figure of merit in excess of 100," in *Proc. 19th Int. Conf. Solid-State Sens., Actuators Microsyst. (TRANSDUCERS)*, Jun. 2017, pp. 1838–1935, doi: 10.1109/TRANSDUCERS.2017.7994447.

Authorized licensed use limited to: ShanghaiTech University. Downloaded on June 01,2023 at 06:29:33 UTC from IEEE Xplore. Restrictions apply.